DENDROBIOLOGY

2026, vol. 95, 170–189

https://doi.org/10.12657/denbio.095.012

Anthony Guerra, Ernesto C. Rodríguez-Ramírez*

Growth and functional trait responses of *Berberis lutea* to Super El Niño events in Peruvian altimontane shrublands

Received: 16 April 2026; Accepted: 29 May 2026

Abstract: Shrubs are key components of high-Andean xeric ecosystems and provide valuable dendroclimatic information where tree records are scarce, yet their responses to extreme El Niño-Southern Oscillation (ENSO) anomalies remain poorly understood. We developed the first shrub-ring chronologies of *Berberis lutea* from two Peruvian altimontane shrublands (San Pedro de Saños and Singua Chico) to evaluate climate-growth relationships and the effects of Super El Niño events on radial growth sensitivity, resilience, and wood anatomical traits. Ring-width chronologies were analysed against temperature, precipitation, evapotranspiration, and Niño 3.4 sea surface temperature anomalies. Resistance, recovery, and resilience indices, together with wood anatomical traits and fourth-corner analyses, were used to assess functional responses during the 1997/98 and 2015/16 Super El Niño events. *B. lutea* formed clear annual rings with strong common signals and high inter-series coherence, confirming its suitability for dendroclimatic studies. Radial growth was mainly driven by temperature, evapotranspiration, and ENSO-related sea surface temperature variability, whereas precipitation showed weaker and site-dependent effects. Notably, a negative precipitation-growth correlation was found at the lower-elevation site (San Pedro de Saños), which we attribute to cloud-cover limitation and transient soil waterlogging – mechanisms that are now explicitly discussed. Super El Niño events caused moderate reductions in radial growth followed by rapid, site-specific recovery, with greater resilience at San Pedro de Saños. These growth responses were accompanied by narrower vessel diameter and reduced vessel length, indicating conservative hydraulic adjustments under extreme climatic stress. Overall, *B. lutea* emerges as a reliable climate proxy and a strong bioindicator of resilience to increasing ENSO-driven climate extremes in high-Andean semi-xeric ecosystems.

Keywords: eco-physiological plasticity, extreme climate events, shrub dendroclimatology, trait acclimation

Addresses: A. Guerra, Universidad Tecnológica del Perú, Huancayo, Perú;
https://orcid.org/0000-0002-9830-8550, e-mail: guerrag.anthony@gmail.com;
E.C. Rodríguez-Ramírez, Facultad de Ciencias Biológicas, Benemérita Universidad Autónoma de Puebla, Pue, Mexico; https://orcid.org/0000-0001-6206-8615, e-mail: chanes.rodriguez@correo.buap.mx
* corresponding author

Introduction

Large-scale ocean–atmosphere teleconnections are among the main drivers of interannual climate variability, linking anomalies in tropical sea surface temperatures with hydroclimatic responses across distant terrestrial ecosystems (Taschetto et al., 2020; Feng et al., 2021). Among these, ENSO is one of the most influential climate modes, altering regional temperature regimes, atmospheric circulation, precipitation patterns, and evapotranspirative demand across tropical and subtropical mountains (Cai et al., 2020; Poveda et al., 2020). In the tropical Andes, ENSO-related anomalies can strongly modify the seasonal water balance, influencing cambial activity, xylem formation, and the long-term growth performance of woody species.

Historical Super El Niño events represent the most extreme expression of ENSO-related interannual climate variability, profoundly influencing the structure, functioning, and resilience of terrestrial ecosystems (Richter & Ise, 2005; Lyu et al., 2018). In tropical regions, these climate events have triggered severe droughts and heatwaves that markedly reduce radial growth and increase mortality in woody species (Rifai et al., 2019; Cai et al., 2020; Groenendijk et al., 2025). Although the intensity of their impacts varies across biomes, climatic contexts, and geographic regions, the cumulative consequences of Super El Niño events can significantly disrupt forest carbon dynamics and compromise the structural stability of diverse ecosystems (Holmgren et al., 2006; Feron et al., 2024).

In response to these challenges, dendroclimatology has emerged as a key discipline for elucidating long-term ecological responses to climate variability and change (Fritts, 1976; Speer, 2010). Although traditionally focused on tree species, its recent expansion to include shrubs represents a promising frontier for extending the spatial and ecological scope of high-resolution dendrochronological records, particularly in high-mountain ecosystems where trees are scarce or absent (Sánchez-Calderón et al., 2022; Portal-Cahuana et al., 2023; Andreu-Hayles et al., 2023). Mounting evidence from high-elevation studies demonstrates that climate exerts a dominant control on plant growth and distribution in highland ecosystems, especially at treeline and shrubline ecotones. In these environments, low temperatures act as the primary limiting factor for woody plant growth at high elevations, where thermal thresholds constrain cambial activity, tissue formation, and reproductive success (Körner, 2012, 2021; Vieira et al., 2026). Consequently, even small variations in growing season temperature can induce significant changes in radial growth, wood anatomy, and shrub establishment patterns. Globally, shrub-based dendrochronological studies in Arctic and alpine regions have revealed strong climatic sensitivity such as high temperature, snow cover, and soil moisture, all of which exert a critical influence on cambial activity (Dobbert et al., 2022; Magnússon et al., 2023; Opała-Owczarek et al., 2024). However, in the xeric and semi-xeric Andes, dendroclimatic and wood anatomical evidence for high-mountain shrubs remains critically scarce. This knowledge gap limits our ability to predict how these species regulate xylem formation and hydraulic function under extreme climatic events, thereby hindering a mechanistic understanding of Andean ecosystem resilience (Rodríguez-Morata et al., 2022; Guerra et al., 2025; Carabajo-Hidalgo et al., 2025).

In this context, the Peruvian altimontane shrublands (henceforth PAS) represent a model ecosystem for high-elevation tropical environments subjected to seasonal water stress. These ecosystems play a critical role in hydrological regulation and soil conservation, acting as natural buffers that capture and gradually release water. Their pronounced climatic variability and steep environmental gradients provide an ideal setting for examining plant hydraulic strategies and climatic sensitivity in tropical mountains (Suárez et al., 2023). They are characterized by cold and relatively dry conditions, with annual precipitation ranging from 250 to 1100 mm and a pronounced seasonality (Aceituno & Garreaud, 2016). This function becomes particularly critical in xeric regions of the country affected by climate change and extreme events such as El Niño (Poveda et al., 2020; Gonzáles et al., 2024).

Among the emblematic taxa of the PAS, the genus *Berberis* L. (Berberidaceae) includes several relict endemic species of the high Andean zones of Peru and Ecuador, often restricted to specific edaphoclimatic conditions (Ulloa et al., 2006, 2025). Multiple *Berberis* species are currently categorized as vulnerable or endangered due to their isolated distribution, habitat fragmentation, and ongoing threats, emphasizing the need for targeted conservation actions (Sarikaya & Uzun, 2024). Within this genus, *B. lutea* Ruiz & Pav. offers a compelling model for dendroclimatic and eco-anatomical research. Anatomically, this multi-stemmed shrub produces well-defined annual growth rings delimited by bands of thick-walled fibers and marginal parenchyma, features that facilitate reliable cross-dating (Carlquist, 1995). Physiologically, its xylem is characterized by small-diameter vessels and high vessel density, a hydraulic architecture associated with drought tolerance and cavitation resistance. These wood anatomical traits, combined with its xeromorphic leaves that terminate in thorns, enable *B. lutea* to maintain cambial activity under the cold, semi-xeric conditions of the high Andes. Together, these characteristics make it a highly suitable indicator species for reconstructing hydroclimatic

variability and assessing the anatomical imprint of extreme climatic events.

Despite the ecological significance of Andean shrublands and the recognized sensitivity of *Berberis* species to environmental gradients, integrative studies combining dendrochronology, wood anatomical traits, and physiological responses to Super El Niño events are virtually absent. This gap is particularly significant given the increasing frequency and intensity of Super El Niño events and their profound impacts on Andean ecosystems. Understanding how xerophytic woody species respond to such extreme climatic pulses is essential for predicting ecosystem stability under future climate change scenarios (Groenendijk et al., 2025; Guerra et al., 2025). Accordingly, the objectives of this study were to: (1) assess the response of *B. lutea* shrub-ring growth to evapotranspiration, monthly precipitation, and variations in mean maximum temperature; (2) analyze the spatial influence of temperature, sea surface temperature, and precipitation; (3) determine the resistance, recovery, resilience, decline phase, and recovery phase of shrub-ring growth under the influence of Super El Niño events; and (4) evaluate the effects of these events on wood anatomical traits across study sites. We hypothesize that *B. lutea* will exhibit reduced radial growth and narrower conductive tissues during Super El Niño years due to intensified drought stress and higher evaporative demand (Medeiros et al., 2025). Specifically, we expect smaller vessel areas but higher vessel frequency, indicating a shift toward hydraulic safety mechanisms. Following these events, we expect compensatory growth recovery and enhanced resilience, reflecting adaptive strategies that maintain functional stability under recurrent climatic extremes.

Methods

Study site

This study was carried out in two PAS dominated by *B. lutea*: San Pedro de Saños (Department of Junín, 11°56'47"S, 75°13'54.6"W; 3,786 m a.s.l.) and Singua Chico (Department of Lima, 12°08'11"S, 75°44'05"W; 4,574 m a.s.l.; Fig. 1a). These sites were selected to capture contrasting microclimatic conditions along an altitudinal gradient, providing a suitable model for assessing the consistency of climate–growth relationships across different elevations. Both sites experience temperate subalpine to cold xeric climates (Cwc, BWk; Peel et al., 2007), with high daily temperature oscillation, a cool dry season (late May to early August), and a wet cool season (early September to late April; Fig. 1b). Mean annual temperature ranges from 10.3 to 11.3 °C and annual precipitation from 942 to 960 mm. Soils are predominantly Leptosol eutrophic–Cambisol eutrophic (LPe-CMe).

The vegetation in these zones is dominated by high Andean shrub thickets (e.g., *Berberis* spp., *Baccharis* spp., *Chuquiraga spinosa* Less., *Minthostachys mollis* Griseb., *Senecio pyrenophilus* Cuatrec., and *Colletia spinosissima* J.F. Gmel.), and Andean grasses such as *Calamagrostis macrophylla* (Pilg.) Pilg., *Stipa* sp., *Poa* sp., *Festuca* sp., and *Parastrephia* sp. (Suárez et al., 2023; Coaguila et al., 2025). The San Pedro de Saños shrubland is subject to moderate anthropogenic influence (logging, grazing, and afforestation with *Eucalyptus globulus* Labill.) in its lower periphery. However, these disturbances primarily affect herbaceous vegetation and shrub species other than *B. lutea*, and all sampled individuals were located in undisturbed patches away from direct human intervention.

Study species

B. lutea (traditional named Ccarhuascassa) is an evergreen Andean shrub well adapted to the semi-xeric conditions of the PAS. It is a multi-stemmed species, typically reaching 0.75 to 3 m in height (Fig. 1c). Its leaves terminate in thorns, a xeromorphic trait that reduces water loss and enables survival under the harsh climatic conditions characteristic of high-elevation environments. These physiological and anatomical adaptations, combined with its well-defined annual growth rings and marked responsiveness to climatic variability, make *B. lutea* a suitable indicator species for dendroclimatological studies in tropical alpine ecosystems.

Sample collection and chronology development

Dendrochronological samples were collected in two PAS dominated by *B. lutea*: 21 individuals from San Pedro de Saños, and 27 from Singua Chico. Two basal stem cross-sections were extracted from each shrub using a hand saw (Total®), approximately 2–5 cm above ground level, considering the multi-stemmed growth habit characteristic of the species (Oladi et al., 2017). In total, 42 and 54 cross-sections were obtained from San Pedro de Saños and Singua Chico, respectively. Individuals showing phytosanitary damage or evident physical alterations associated with fire, grazing, or logging were excluded.

Cross-sections were air-dried at room temperature for approximately one week and subsequently sanded with a progressive sequence of coarse grit sandpapers (120, 180, 220, 240, 320, 420, 600 and 800 grit) until a polished surface allowed clear visualization of annual growth rings (Fig. 1d1, 2; Orvis & Grissino-Mayer, 2002). Shrub-ring dating was

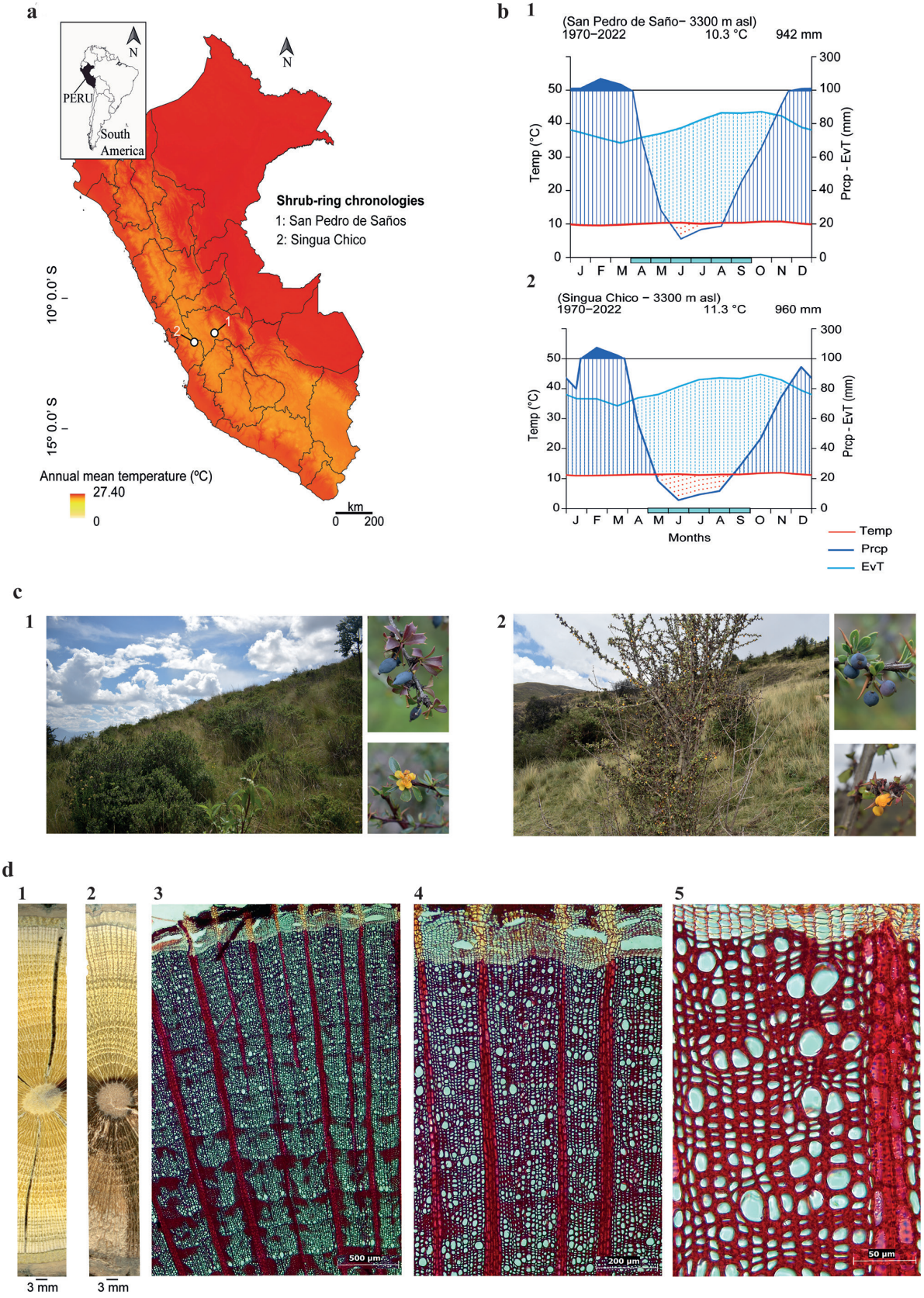

Fig. 1. Study area and general characteristics of *B. lutea*. (a) Location map of the two study sites (San Pedro de Saños and Singua Chico) with annual mean temperature scale. (b) Climograms for (b1) San Pedro de Saños and (b2) Singua Chico. (c) *B. lutea* individuals in their natural habitat: (c1) San Pedro de Saños and (c2) Singua Chico; fruits and flowers are visible. (d) Growth rings: (d1) San Pedro de Saños and (d2) Singua Chico; (d3–d5) transverse anatomical sections at increasing magnifications: 40× (d3), 100× (d4), and 400× (d5)

performed by assigning calendar years according to Schulman (1956) convention for the Southern Hemisphere. The ring widths were measured under a stereomicroscope (OMAX®) using MeasureJ2X software and a Velmex Measuring System (Velmex Inc., Bloomfield, NY, USA) with a precision of 0.001 mm. Verification of false or missing rings, as well as cross-dating among individual series, was conducted with the COFECHA software (Grissino-Mayer, 2001), which calculates Pearson correlation coefficients (*r*) in 30-year segments with a 15-year overlap and a 99% significance level (Holmes, 1983).

To obtain standard *B. lutea* Ring-Width Index (RWI) that preserves the high-frequency signal (Speer, 2010). We standardized the raw ring-width data by fitting an exponential curve for each individual RWI series to remove autocorrelation and ontogeny effects using the software R with the dplR package (Bunn, 2008). The quality of the chronology was assessed using the expressed population signal (EPS >0.85; Briffa, 1990) as a measure of the total signal present in the chronology and the mean correlation coefficient (Rbar) among the RWIs (Wigley et al., 1984).

Identification and delimitation of Super El Niño events in shrub-rings

Considering wood quality, series length, mean sensitivity (MS > 0.2; Speer, 2010), and correlation with the master chronology, we selected five transverse sections from each study site for quantitative wood anatomical analyses of *B. lutea*. From these dated samples, we focused on the four years associated with Super El Niño events (1997/98 and 2015/16; Richter & Ise, 2005; Lyu et al., 2018), together with the two years preceding (1995/96 and 2013/14) and the two years following each event (1999/2000 and 2017/18). This design provided six annual rings per event window for each sample, resulting in a total of 60 shrub rings per study site. The sample size is consistent with recent studies investigating shrub anatomical traits and plant water potential during extreme climatic events (five samples; Ganthaler & Mayr, 2021; Guerra et al., 2024).

Rather than capturing a single image representing an entire section, the annual rings corresponding to each target year were individually digitized from the transverse sections using a Leica® microscope (DM1000) equipped with a Leica® camera (ICC50 W) (Fig. 1d3-5). Although multiple annual rings were present within the same transverse section, each target ring was imaged separately to standardize the quantification of vessel and ray traits at the annual scale and to avoid anatomical variation that could confound comparisons among adjacent years. Each ring image encompassed approximately six wood rays, averaging 0.42 mm in width and 0.95 mm in length. The acquired images were stored in TIFF format at a resolution of 1.3 μm per pixel.

Climate-growth correlations

To identify the climate signal on *B. lutea* shrub-rings, we assessed the influence of the monthly evapotranspiration, precipitation, and temperature (maximum, minimum and average) data for a common period (1986-2022) obtained from the CHELSA database (http://chelsa-climate.org/; Karger et al., 2021), the layer resolution was c. 1 km^2; and SST 3.4 (1986–2022) from the nearest Climatic Research Unit grid cell (CRU TS 4.0.6; https://climexp.knmi.nl/). We analyzed the relationships between the *B. lutea* RWI and climatic variables using Pearson's correlation coefficient (*r*) with the corrplot R package (Wei & Simko, 2010). To determine whether growth is influenced by specific climatic variations, the relationships between climate and growth were examined over a 24-month period, spanning from May to August (dry season) and from September to April (rainfall season), which may influence ring growth (Fritts, 1976).

Spatial correlations of shrub growth variations

To assess the spatial correlations between the *B. lutea* shrub-ring time series and several climate variables (e.g., maximum and minimum temperature, precipitation, sea surface temperature, and vapour pressure), we used the KNMI Climate Explorer based on the CRU TS 4.06 dataset (spatial resolution: 0.5°; Trouet & Van, 2013). The climate data were extracted separately for each study area. Monthly windows were selected according to the local precipitation seasonality and the period of active shrub growth to better capture the effects of regional climatic oscillations on shrub-ring variability.

Sensitivity of ring width to Super El Niño events

To determine the effects of Super El Niño events on the RWIs in each study area, we calculated three sensitivity indicators for each RWI: resistance (Rt; Eq. 1), recovery (Rc; Eq. 2), and resilience (Rs; Eq. 3). Additionally, we assessed two phases of past shrub growth depression (SGD): decline phase (DecU; Eq. 4) and recovery phase (RecU; Eq. 5) (Mu et al., 2022), defined as follows:

$$Resistance\ (Rt) = \frac{Ring\ width_t}{Ring\ width_{t-2}} \quad (1)$$

$$Recovery\ (Rc) = \frac{Ring\ width_{t+2}}{Ring\ width_t} \quad (2)$$

$$Resilience\ (Rs) = \frac{Ring\ width_{t+2}}{Ring\ width_{t-2}} \quad (3)$$

$$Decline\ phase\ (DecU) = \frac{Pre5 - Min}{Dt} \quad (4)$$

$$Recovery\ phase\ (RecU) = \frac{Post5 - Min}{Rt} \quad (5)$$

where Ring width$_t$ is the annual ring width of *B. lutea* in year *t*, Ring width$_{t-2}$ and Ring width$_{t+2}$ correspond to the mean ring width of the two years preceding and following year *t*, respectively. Pre5 and Post5 were calculated by averaged RWIs of five years before and after a SGD, respectively, representing pre- and post-stress growth conditions. Min is the minimum RWI during a SGD; whereas Dt and Rt are the number of years covered by decline and recovery phases of a SGD (Mu et al., 2022). We calculated individual shrub-level indices and rate for selected years during the period 1995–2000 and 2013–2018. The differences in ring width among Super El Niño events and study areas were tested using two-way repeated-measures ANOVA with pairwise *post-hoc* comparisons. Statistical analyses were performed in R using the vegan package (Oksanen et al., 2019), whereas data visualization was conducted with ggplot2 (Wickham et al., 2021).

Wood anatomical traits

Wood Anatomical: Four wood anatomical traits were analyzed from a sample of five *B. lutea* individuals, previously described for the identification and delimitation of Super El Niño events: (1) hydraulic diameter (D_H), (2) vessel length (V_L), (3) fiber lumen diameter (F_{LT}), and (4) fiber total diameter (F_{WW}) (Table 1; Fonti et al., 2025).

The selected rings were immediately fixed in a solution of formalin, acetic acid and ethanol (10:5:85) (McCracken & Johansen, 1940). Subsequently, they were washed with tape water and stored in a solution of glycerin and water (1:1) for 15 days for softening and subsequent preparation of cross-sections. Likewise, duplicate samples of the selected rings were prepared by maceration through wood chips, to quantify the traits of the vessels and fibers. Cross-sections were obtained with a Leica® SM2010R microtome and rinsed in 20% NaClO solution. For dehydration, sections were immersed in a progressive series of ethanol solutions (20%, 50%, 70%, and 100%), with immersion lasting 5 minutes at each concentration. Staining was performed with 1% hydroalcoholic safranin for 5 minutes. Finally, sections were fixed in a 1:1 alcohol:acetate ratio for 5 minutes and permanently mounted on histological slides using synthetic resin.

For the preparation of the macerates, wood chips were placed in a 1:1 mixture of glacial acetic acid and hydrogen peroxide at 70 °C for 48 h (Franklin, 1945). Subsequently, the chips were washed with distilled water. Finally, the chips were stained with 1% hydroalcoholic safranin and semi-permanently mounted on histological slides using 50% glycerinated water.

For the analysis of wood anatomical characteristics, high-resolution images (1.3 μm per pixel) were obtained following the recommendations of the International Association of Wood Anatomists (IAWA Committee, 1989). A Leica® DM1000 optical microscope coupled to a Leica® ICC50 W camera was used for image acquisition. Image processing and quantification of vessel and fiber characteristics were performed using ImageJ software (Media Cybernetics, Silver Spring, MD, USA).

Statistical differences in quantitative wood anatomical traits were assessed using a one-way analysis of variance (ANOVA) followed by Tukey's *post-hoc* test, implemented in the R environment. Statistical analyses were carried out using base R functions and the vegan package (Oksanen et al., 2019), while graphical representations were generated with ggplot2 (Wickham et al., 2021).

Table 1. Overview of functional traits, their acronyms, variable units, and ecophysiological function

Trait type	Functional traits	Acronym	Variable unit	Ecophysiological function
Wood anatomical	Hydraulic diameter	D_H	μm	Optimizing water transport efficiency and ensuring hydraulic safety in plants (Fonti et al., 2025).
	Vessel length	V_L	μm	Associated with acclimatization and optimizing xylem functionality to survive in adverse conditions (Fonti et al., 2025).
	Fiber lumen diameter	F_{LT}	μm	It balances water conduction and the mechanical strength of the wood (Fonti et al., 2025).
	Fiber total diameter	F_{WW}	μm	It is associated with the mechanical strength and flexibility of wood (Fonti et al., 2025).

Effect of climate on wood anatomical traits

A model-based fourth-corner analysis was employed to examine correlations between wood anatomical traits and climatic conditions during Super El Niño and non-Super El Niño years. This approach addresses the fourth-corner problem by analyzing relationships among three matrices: (1) species occurrence across geographical sites, (2) species × traits, and (3) sites classified by Super El Niño and non-Super El Niño years, to estimate trait–hydric stress associations (Borcard et al., 2011). We followed the framework of Warton et al. (2015), implemented in the R package mvabund (Wang et al., 2012). This method involves fitting a Generalized Linear Model (GLM) with climatic variables as predictors and their interactions with functional traits. To improve model fit, we used a Poisson distribution for errors and applied LASSO penalization using the mvabund package (Wang et al., 2012). The model was evaluated using diagnostic plots to assess its accuracy. All analyses were conducted using the fourth-corner function in the R package ade4 (Dray & Dufour, 2007).

Results

Shrub-ring width chronology

This study demonstrates the first ring-width chronologies of *Berberis lutea* from the PAS of San

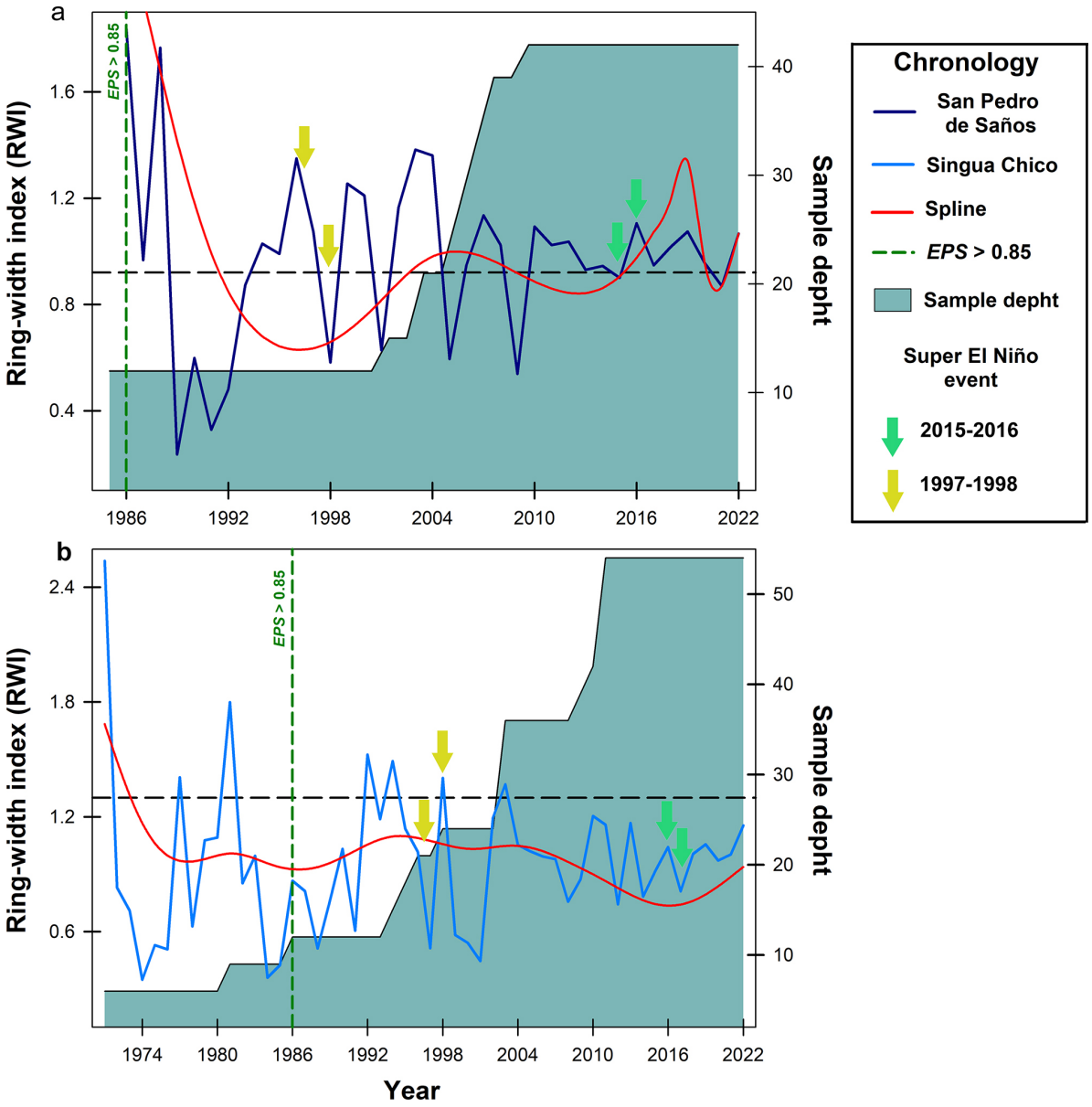

Fig. 2. Shrub-ring width chronologies of *B. lutea* for: San Pedro de Saños (a) and Singua Chico (b). Arrows represent specific Super El Niño events (1997–1998 and 2015–2016)

Table 2. Statistical analysis of the reference chronologies of *Berberis lutea* in peruvian altimontane shrublands

Statistics	San Pedro de Saños	Singua Chico
Number of individuals analyzed (series)[a]	21 (42)	27 (54)
Time span (years)[a]	1986–2022 (37)	1971–2022 (52)
Mean ring width (mm/year)[b]	0.52	0.54
Mean series intercorrelation coefficient[a]	0.73	0.64
Average mean sensitivity[a]	0.45	0.43
Mean EPS[b]	0.88*	0.93*
Mean R_{bar} [b]	0.56	0.51

[a] Values obtained using the COFECHA program (Holmes 1983)
[b] Values obtained from the standard chronology with the R-studio program using the dplR package (Bunn 2008).
* The EPS (expressed population signal) must present a value ≥0.85, which is an appropriate cutoff point; in this case, it is above the value.

Pedro de Saños and Singua Chico, covering 37 years (1986–2022) and 52 years (1971–2022), respectively. *B. lutea* exhibited distinctive annual growth rings, characterized by vessel elements arranged in a semi-ring-porous pattern, delimited by a line of large vessels at the beginning of early wood, and with axial and radial parenchyma distributed in bands surrounding the vessels (Fig. 1d).

Standard dendrochronological statistics confirmed the reliability of the shrub-ring chronology analysis (Fig. 2; Table 2). Interseries correlations were consistently high in both sites, with values ≥ 0.64 (Table 2). The mean sensitivity (MS) revealed a pronounced year-to-year variability (MS ≥ 0.43; Table 2). The expressed population signal (EPS) exceeded the commonly accepted threshold of 0.85 in both chronologies (EPS ≥ 0.88; Table 2). Likewise, the mean interseries correlation (Rbar) was higher than 0.50 (Table 2), indicating strong coherence among individuals and a robust common signal within the chronology.

Climatic correlations on shrub-ring width

Pearson's correlation analysis between the RWI of *B. lutea* and local climatic variables for the period 1986–2022 revealed significant contrasts between the two study sites, with distinct responses to climatic drivers across previous and current growth years (Fig. 3).

In San Pedro de Saños, maximum temperature (Tmax) was positively correlated with radial growth during both the previous rainfall season (November–December; r = 0.431–0.417) and the current growing year (November–December; r = 0.434–0.407), with an additional positive association in February (r = 0.372). Similarly, in Singua Chico, Tmax showed consistent positive correlations with growth during the previous growth cycle, particularly in June (r = 0.372), September (r = 0.347), January (r = 0.441), and April (r = 0.326) (Fig. 3a).

Regarding minimum temperature (Tmin), San Pedro de Saños exhibited a significant negative correlation during October of the previous year (r = −0.335), which became even stronger in October of the current year (r = −0.443). In contrast, Singua Chico showed positive Tmin growth relationships mainly during the previous dry season (June; r = 0.373) and the preceding rainfall season, particularly in September–October (r = 0.355–0.415), with another positive signal in April (r = 0.325) (Fig. 3b).

For precipitation, San Pedro de Saños showed a significant positive correlation during the previous rainfall season, specifically in April (r = 0.326). However, negative correlations dominated the current growth period, especially during the dry season (June: r = −0.455; August: r = −0.345) and again in the rainfall season (November: r = −0.451). In Singua Chico, positive precipitation growth correlations were detected during both the previous dry season (July: r = 0.372) and the previous rainfall season (October: r = 0.356). A similar pattern was observed during the current growth year, with significant positive correlations in July (r = 0.327) and October (r = 0.349) (Fig. 3c).

Evapotranspiration (EvT) in San Pedro de Saños was positively associated with growth across most months of both the previous and current growth periods. During the previous dry season, positive correlations extended from August to October (r = 0.386–0.495), while during the previous rainfall season they intensified from November to February (r = 0.506–0.643). A comparable trend was observed during the current year, with positive correlations during the dry season (July–September; r = 0.337–0.424) and the rainfall season (October–February; r = 0.539–0.628). By contrast, Singua Chico displayed negative EvT growth correlations during the previous rainfall season (February: r = −0.347) and the current rainfall season (April: r = −0.461) (Fig. 3d).

Finally, in San Pedro de Saños, sea surface temperature anomalies in the Niño 3.4 region (SST 3.4) were positively related to growth during the previous year only in May (r = 0.479). In the current growth period, however, positive correlations were observed across most months, spanning from the dry season (June–July; r = 0.462–0.405) through the rainfall season (November–May; r = 0.331–0.329). In contrast, Singua Chico showed strong and persistent positive correlations throughout all months of the previous growth cycle (June to May), with coefficients ranging from r = 0.331 to 0.530 (Fig. 3e).

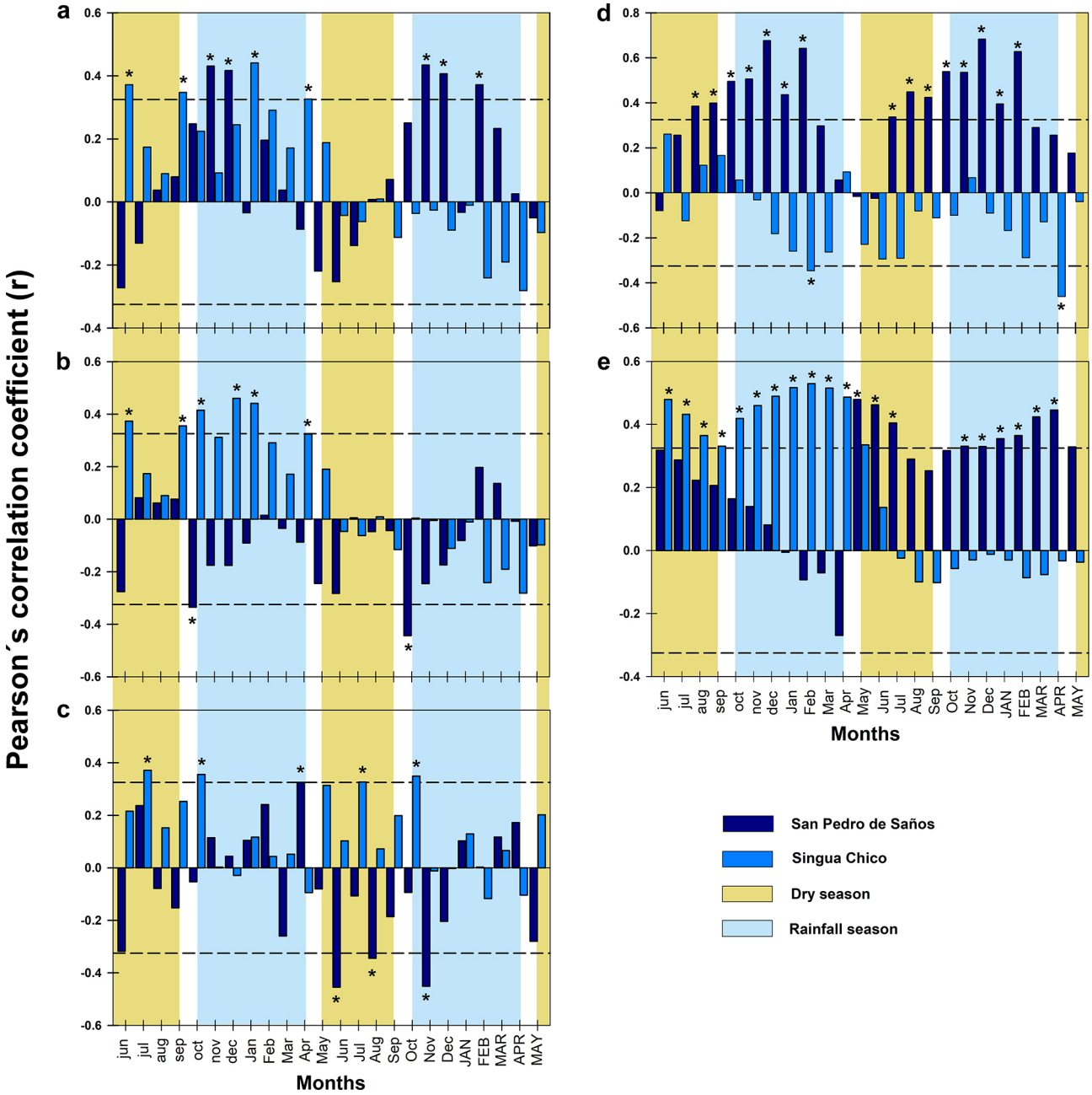

Fig. 3. Pearson correlation coefficients (r) between *B. lutea* ring-width index (RWI) chronologies and climatic variables, including mean maximum temperature (a), mean minimum temperature (b), monthly precipitation (c), evapotranspiration (d), and Niño 3.4 sea surface temperature (SST) (e), over the common period 1986–2022 (n = 37; two-tailed critical r = 0.325) for each study site. Horizontal dashed lines denote the significance level ($p < 0.05$)

Spatial correlations on shrub growth

The spatial correlations with different climatic parameters (i.e., maximum and minimum temperature, precipitation, sea surface temperature, and vapour pressure) exhibited that the strongest positive and negative correlations were related to maximum and minimum temperature, precipitation, sea surface temperature, and vapour pressure between study sites (Fig. 4). Positive correlations exhibited gradual changes throughout the chronologies. The spatial field correlation between Tmax and Singua Chico chronology (from January to April) covered a larger area in Singua Chico chronology stretching to central Peru (r = 0.4, $p < 0.05$; Fig. 4a), whereas the San Pedro de Saños chronology (from October to November) covered a smaller area (r = 0.2, $p < 0.05$; Fig. 4b). Likewise, Singua Chico chronology showed a strong correlation (r = 0.5, $p < 0.05$; Fig. 4c) with Tmin; but differing in San Pedro de Saños chronology exhibiting a negative correlation (r = −0.2, $p < 0.05$) from June to July; Fig. 4d). Notably, both

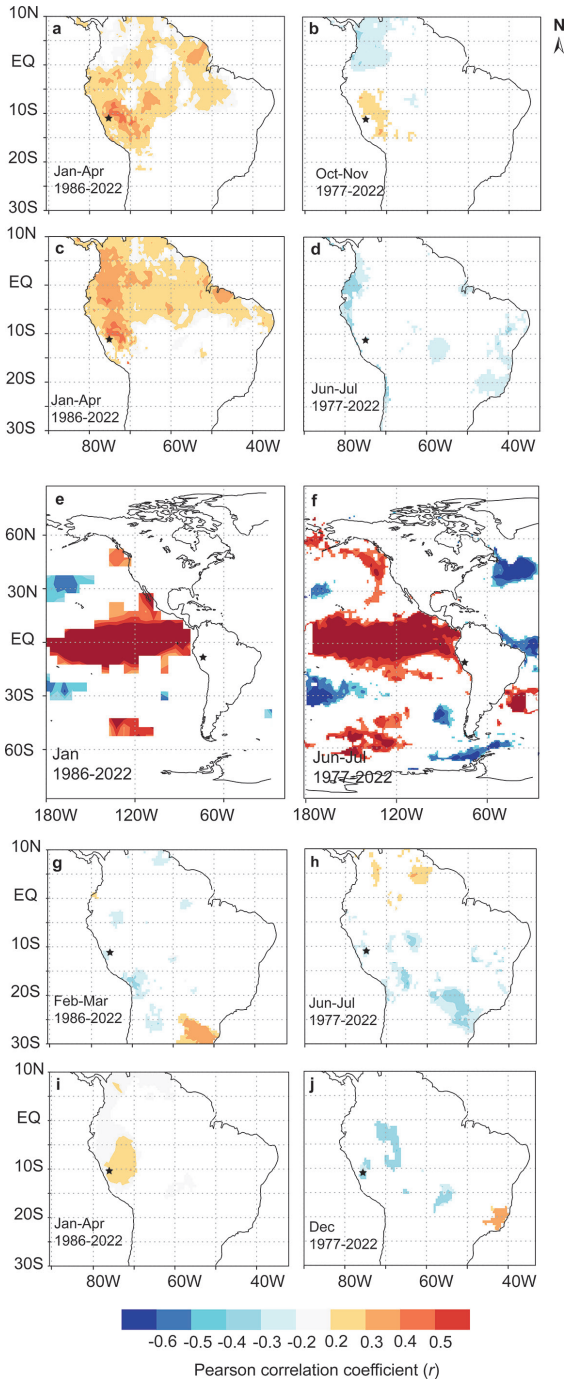

Fig. 4. Significant spatial correlation ($p < 0.05$) between *B. lutea* RWI chronologies and climatic variables: significant relationships were found for maximum temperature in January-April (Singua Chico; a) and October-November (San Pedro de Saños; b); for minimum temperature in January-April (Singua Chico; c) and June-July (San Pedro de Saños; d); for sea surface temperature (SST) in January (Singua Chico; e) and June-July (San Pedro de Saños; f); for precipitation in February-March (Singua Chico; g) and June-July (San Pedro de Saños; h); for vapor pressure in January-April (Singua Chico; i) and December (San Pedro de Saños; j). Climate data were extracted from KNMI Climate Explorer (CRU TS 4.06 dataset, spatial resolution in 0.5° bins; https://climexp.knmi.nl/; Trouet & Van, 2013)

site chronologies were positively associated with SST variability. In Singua Chico, the relationship was significant in January ($r = 0.500$, $p < 0.05$; Fig. 4e), whereas in San Pedro de Saños significant positive correlations extended from June to July ($r = 0.500$, $p < 0.05$; Fig. 4f). Although the two species showed significant negative correlations with Prec ($r = -0.2$, $p < 0.05$; Fig. 4g, h), Singua Chico chronology was linked from February to March, whereas San Pedro de Saños chronology was related from June to July. Last, Singua Chico chronology showed a positive correlation with vapour pressure from January to April ($r = 0.5$; $p < 0.05$; Fig. 4i) and negative correlation in December for San Pedro de Saños chronology ($r = -0.3$; $p < 0.05$; Fig. 4j).

Ring-width sensitivity to Super El Niño events

The Super El Niño event had a clear impact on the radial growth sensitivity of *B. lutea* at both study sites. The high values of resistance, recovery, and resilience, together with positive decline phase and variable recovery phase values, indicate that the species exhibits a strong capacity to tolerate severe drought conditions and to re-establish growth following disturbance (Fig. 5).

In San Pedro de Saños, resistance (Rt) values ranged from 0.239 to 2.702 (1.054 ± 0.600; mean ± SD), whereas in Singua Chico, they varied from 0.262 to 2.812 (mean = 0.953 ± 0.569). These results reflect a notable stability of radial growth during the stress period, particularly in populations located at intermediate elevations (Fig. 5a). Recovery (Rc) also showed distinct patterns between PAS. In San Pedro de Saños, mean Rc values (1.270 ± 0.763) were higher than those observed in Singua Chico (0.833 ± 0.398), suggesting a more efficient compensatory response following the initial growth reduction (Fig. 5b). Similarly, resilience (Rs) was high at both sites (San Pedro de Saños = 1.205 ± 0.842; Singua Chico = 0.767 ± 0.625), indicating that individuals were able to restore or even exceed their pre-event growth rates (Fig. 5c).

The decline phase in growth (DecU) exhibited low but positive values in both sites (San Pedro de Saños = 0.110 ± 0.132; Singua Chico = 0.160 ± 0.133), suggesting a moderate reduction in growth immediately after the climatic anomaly, followed by gradual recovery (Fig. 5d). In contrast, the recovery phase (RecU) displayed variation: in San Pedro de Saños, mean values were negative (−0.0003 ± 0.050), reflecting greater resilience and potential ecological memory to stress; whereas in Singua Chico, positive values (0.035 ± 0.077) indicated a slower recovery after disturbance (Fig. 5e).

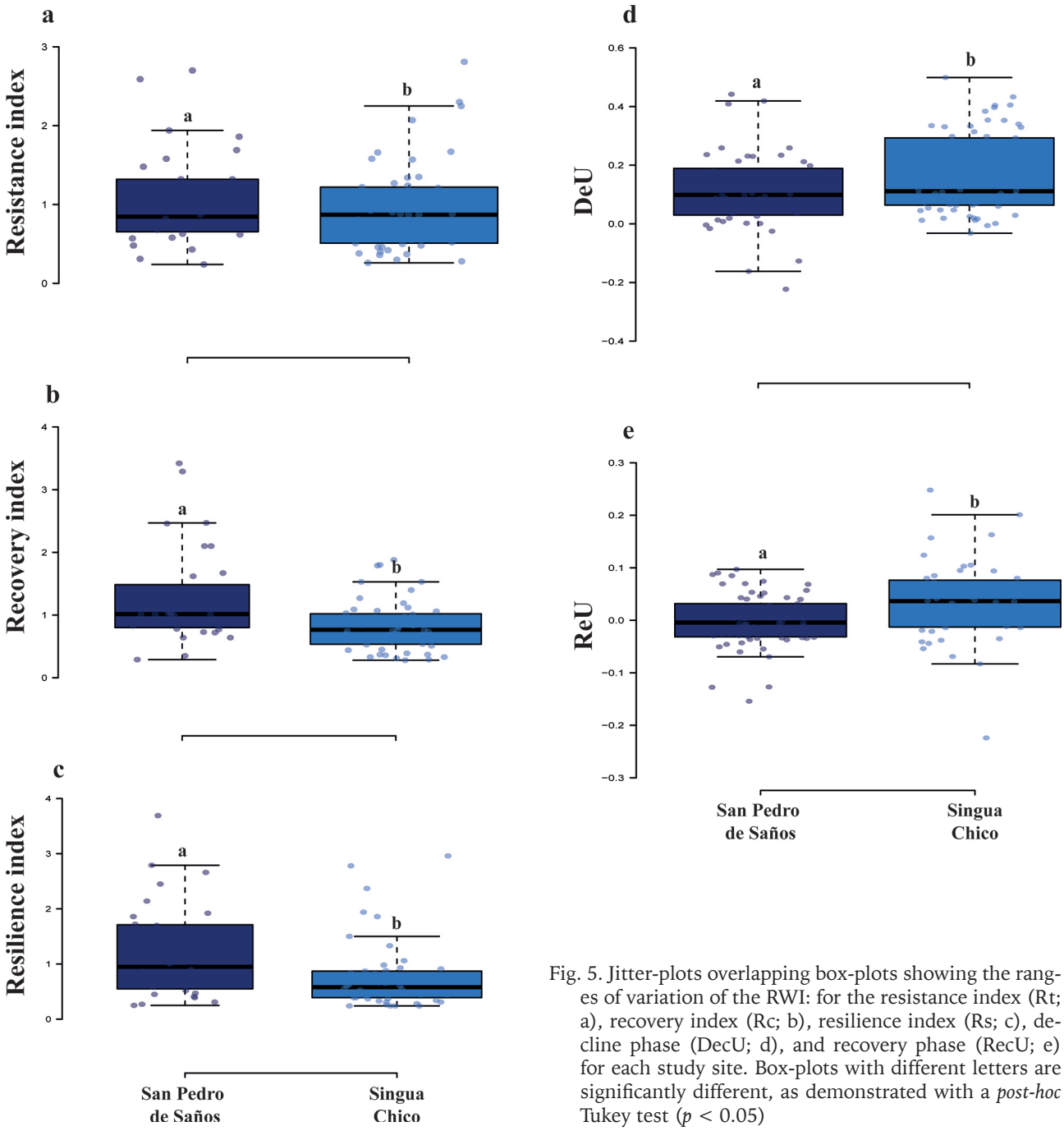

Fig. 5. Jitter-plots overlapping box-plots showing the ranges of variation of the RWI: for the resistance index (Rt; a), recovery index (Rc; b), resilience index (Rs; c), decline phase (DecU; d), and recovery phase (RecU; e) for each study site. Box-plots with different letters are significantly different, as demonstrated with a *post-hoc* Tukey test ($p < 0.05$)

Wood anatomical traits variation

When related specific wood anatomical (D_H and V_L) values for Non-Super El Niño events were significantgly higher (D_H, from14 to 23 μm; and V_L, from 200 to 400 μm) in both study forests (Fig. 6a, b), whereas during Super El Niños events, the D_H and V_L displayed narrow values (D_H, from ≈ 5 to 7 μm; and V_L, from 150 to 300 μm respectively) (Fig. 6a, b). Notwitstanding, during Non-Super El Niño events, the fiber total diameter (F_{WW}) exhibited significant differences between study sites, San Pedro de Saños showed high F_{WW} values (from ≈21 to 27 μm), whereas Singua Chico demonstrated narrower F_{WW} values (from ≈15 to 18 μm; Fig. 6c), whereas during Super El Niño events, the F_{WW} showed high values in both study sites (from 28 to 35 μm; Fig. 6c). Finally, no clear trait variations were observed regarding fiber lumen diameter (F_{LT}) during Non-Super El Niño events, and Super El Niño events between study sites (Fig. 6d).

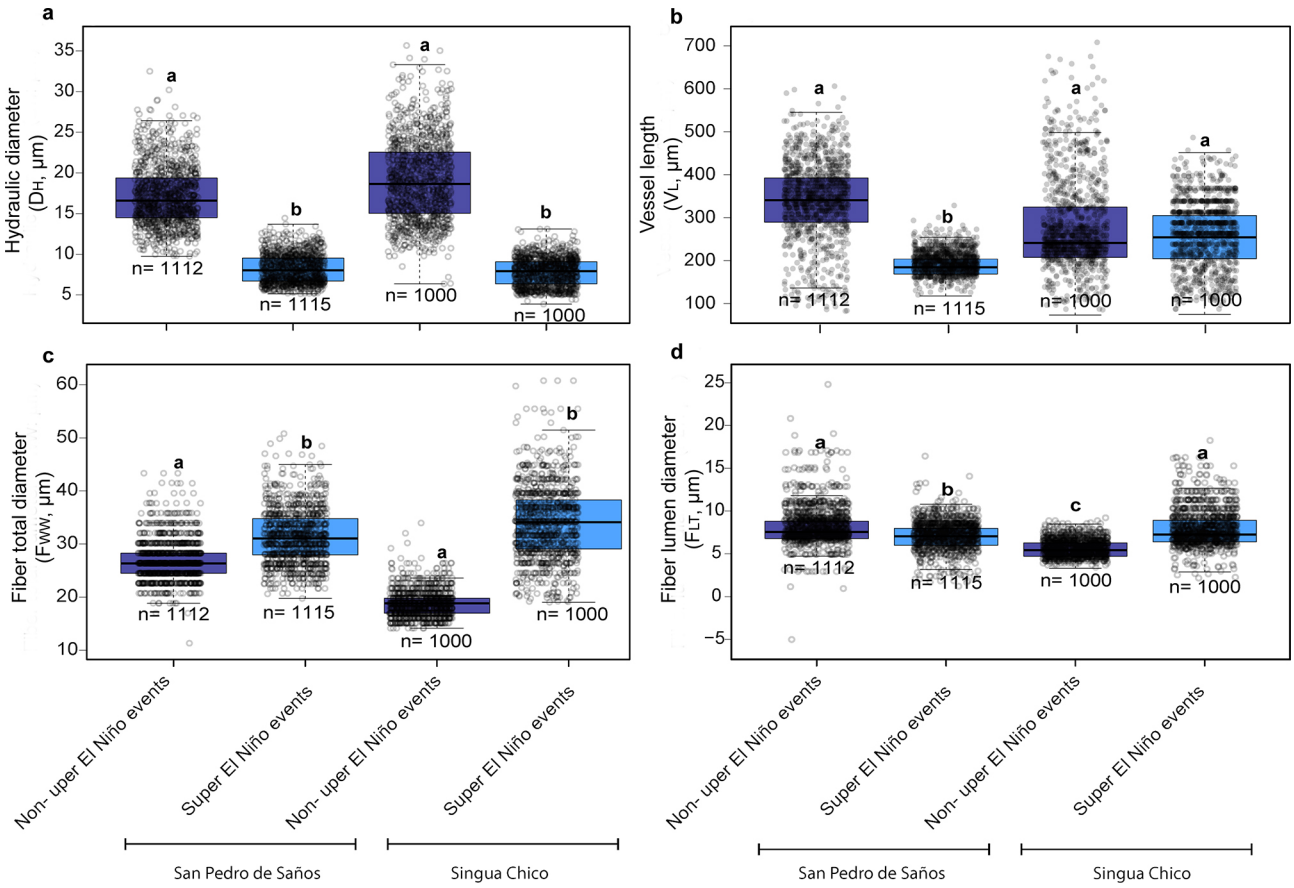

Fig. 6. Jitter-plots overlapping box-plots showing the ranges of wood anatomical trait variation for each study site among Non-Super El Niño events and Super El Niño events. Hydraulic diameter (D_H; a), vessel length (V_L; b); fiber total diameter (F_{WW}; c) and fiber lumen diameter (F_{LT}; d). Box-plots with different letters are significantly different, as demonstrated with a *post-hoc* Tukey test ($p < 0.05$)

Effect of climate on wood anatomical traits

For the fourth-corner analyses utilizing the climatic factors, 689 correlations significantly differed from zero, with an inertia of the overall model of 9567 ($p < 0.001$). In San Pedro de Saños most *B. lutea* wood traits and Super El Niño years were significantly correlated with at least one other trait; D_H, V_L and F_{WW} were negatively correlated during Super El Niño years (i.e., 1997, 1998, 2015 and 2016), whereas during Non-Super El Niño years (i.e., 1995, 1996, 1999, 2000, 2013, 2014, 2017, and 2018) both positive and negative but low correlations were observed (Fig. 7a).

Notwithstanding, Singua Chico displayed high negative correlation during Super El Niño years among wood traits (D_H, V_L, F_{LT} and F_{WW}) (−0.05, Fig. 7b). Nonetheless, F_{LT} demonstrated positive correlation during a Non-Super El Niño year (1995).

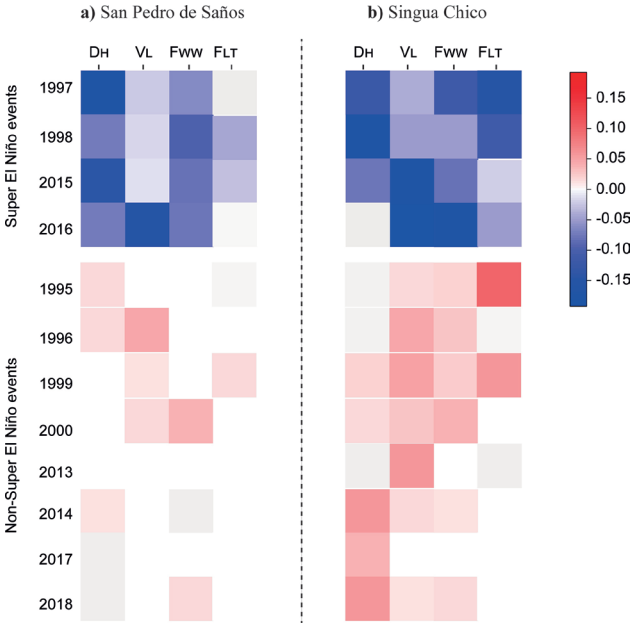

Fig. 7. Results of the fourth-corner analysis. Significant correlations between wood anatomical traits and (a) San Pedro de Saños and (b) Singua Chico during Super El Niño and Non-Super El Niño years. Coloured squares indicate significant correlations ($p < 0.05$). Darker colours represent stronger correlations (positive in red, negative in blue). Wood anatomical traits: hydraulic diameter (D_H), vessel length (V_L), fiber lumen diameter (F_{LT}) fiber total diameter (F_{WW})

Discussion

Shrub-ring width chronology

Berberis lutea exhibited well-defined annual growth rings characterized by vessel elements arranged in a semi-ring-porous pattern. These anatomical traits are consistent with those reported for other *Berberis* species, including *B. lyceum* Royle (Sahney & Tripathi, 2020), *B. moranensis* Schult. & Schult. f. (Ruiz-Valencia et al., 2022), and *Berberis* spp. (Carlquist, 1995), highlighting the structural uniformity and ecological adaptability of the genus.

Standard dendrochronological statistics indicate that the *B. lutea* chronologies are robust and ecologically meaningful, suggesting that radial growth is primarily modulated by interannual climatic variability. High mean sensitivity, together with elevated expressed population signal (EPS > 0.85) and mean inter-series correlation (Rbar), points to a coherent population-level response and a well-resolved common signal, while reducing the influence of individual growth variability. Comparable levels of signal strength have been reported for other high-elevation Andean shrub species, supporting the potential of woody shrubs as climate proxies in mountain environments (Hadad et al., 2022; Rodríguez-Morata et al., 2022; Melián et al., 2024; Guerra et al., 2025). Overall, these findings suggest that shrub-based chronologies can contribute meaningfully to assessments of climate–growth relationships in climatically sensitive ecosystems.

Climatic signal on shrub-rings

Radial growth of *Berberis lutea* showed clear site-specific climatic sensitivity, reinforcing the idea that shrub-ring formation in the tropical Andes is controlled by local thermal thresholds, moisture balance, and lagged physiological responses (Rodríguez-Morata et al., 2022; Portal-Cahuana et al., 2023; Guerra et al., 2025). The contrasting signals between San Pedro de Saños and Singua Chico likely reflect differences in microsite water availability, topographic exposure, cloud cover, and the degree of thermal limitation.

At San Pedro de Saños, the positive relationship between Tmax and growth during the previous and current rainfall seasons suggests that temperature acts as a growth-limiting factor, particularly when soil moisture is adequate (Ganthaler & Mayr, 2021; Rodriguez-Caton et al., 2021). Under these conditions, warmer temperatures may enhance cambial activity, carbon assimilation, and cell maturation, supporting the temperature-threshold hypothesis widely reported for high-elevation Andean vegetation (Macek et al., 2009; García-Plazaola et al., 2015). In Singua Chico, the positive Tmax signal during the previous growth cycle points to a carry-over effect, where warmer conditions may increase non-structural carbohydrate storage that later supports ring formation (Opała-Owczarek et al., 2024; Carabajo-Hidalgo et al., 2025). The Tmin response further supports this mechanism. Negative correlations in October at San Pedro de Saños likely indicate that abrupt nocturnal cooling during the dry-to-rainfall transition constrains cambial reactivation cambium (Hoch & Körner, 2005; Azócar et al., 2007; Carabajo-Hidalgo et al., 2025). By contrast, the broadly positive Tmin signal in Singua Chico suggests that warmer nights reduce cold limitation and favor xylem differentiation and sustained metabolic activity, which are highly temperature-sensitive processes in high-Andean woody plants (Jandova & Dolezal, 2025; Dusenge et al., 2025).

A particularly counterintuitive result emerged at San Pedro de Saños, where precipitation correlated negatively with radial growth during the current growing season, most notably in November ($r = -0.451$), which marks the onset of the rainy season. While water availability is typically limiting in semi-xeric ecosystems, this negative relationship can be explained by site-specific microclimatic and vegetation characteristics. San Pedro de Saños, located at 3,786 m a.s.l., is influenced by a higher density of tree species in its lower periphery, particularly *Alnus acuminata* Kunth and *Escallonia* spp. These species are typically associated with riparian zones and areas of higher soil moisture, and their presence contributes to greater local humidity and more frequent cloud immersion compared to the drier Singua Chico site. During the rainy season, increased cloud cover substantially reduces incoming solar radiation, limiting photosynthetic carbon gain despite abundant soil moisture a phenomenon widely documented in tropical montane cloud forests (Graham et al., 2003; Bruijnzeel et al., 2011; Wilson & Jetz, 2016). This "cloud-growth" effect is further supported by recent reviews demonstrating that persistent cloudiness reduces both photosynthetically active radiation and leaf temperatures, thereby suppressing net carbon assimilation and cambial activity (Hughes et al., 2024; Dusenge et al., 2025). In addition, high rainfall intensity during November may lead to transient soil waterlogging and oxygen deprivation in the rhizosphere, further constraining root respiration and nutrient uptake (Bruijnzeel & Veneklaas, 1998; Carabajo-Hidalgo et al., 2023). The negative precipitation signal observed in June and August further supports this interpretation, as these months coincide with the dry season in the Peruvian Andes; however, at San Pedro de Saños, the presence of cloud immersion sustained by local tree cover and topographic position may maintain high humidity and reduce solar

radiation even during months of low rainfall, dampening growth despite otherwise favorable temperatures. Together, these mechanisms provide a robust biological explanation for the seemingly paradoxical negative correlation between precipitation and radial growth at this site.

In contrast, Singua Chico displayed positive precipitation–growth correlations during both the previous and current growing seasons, consistent with the expectation that soil moisture availability is the primary growth-limiting factor in this drier, higher-elevation site (4,574 m a.s.l.). The absence of dense tree cover and the lower humidity at Singua Chico reduce the likelihood of cloud-induced growth suppression, allowing precipitation to directly enhance cambial activity and ring formation.

EvT signals reveal a shift in climatic constraint between sites: from water supply to atmospheric demand. At San Pedro de Saños, positive EvT correlations indicate that higher EvT reflects energetically favorable conditions, not drought stress, likely because soil moisture remains sufficient (Ganthaler & Mayr, 2021; Pumijumnong et al., 2023; Magnússon et al., 2023). In contrast, negative EvT correlations at Singua Chico point to hydraulic limitation, where increased atmospheric demand reduces turgor and constrains radial growth (Dobbert et al., 2022; Mosquera et al., 2024; De Moura et al., 2025). This contrast supports that evapotranspiration-driven hydraulic stress is more locally mediated than temperature limitation in tropical mountain shrubs.

Finally, the strong positive SST 3.4 signal, especially the persistent response in Singua Chico, highlights the importance of ENSO-driven hydroclimatic forcing. Warm Pacific anomalies likely modulate local temperature and seasonal moisture timing, producing lagged effects on carbohydrate accumulation, cambial priming, and subsequent growth (Pumijumnong et al., 2023). Similar ENSO-growth linkages have been documented in other high-Andean woody species, where ocean–atmosphere variability strongly regulates radial increment through both thermal and hydraulic pathways (Crispín-DelaCruz et al., 2022; Morales et al., 2023; Guerra et al., 2025).

Sensitivity of ring widths to Super El Niño

Although the influence of El Niño oscillations on ring-width variability in some high-Andean species is well established (Crispín-DelaCruz et al., 2022; Morales et al., 2023; Guerra et al., 2025), the anatomical and functional acclimation of xerophytic shrubs to extreme events such as Super El Niño remains incompletely resolved (Sánchez-Calderón et al., 2022; Groenendijk et al., 2025). Our results show that *B. lutea* exhibits coordinated changes in Rt, Rc, Rs, DecU and RecU, indicating that the impacts of Super El Niño extend beyond reduced radial growth and involve functional adjustments linked to stress tolerance and recovery. The high growth sensitivity of *B. lutea*, combined with rapid post-disturbance Rc, is consistent with Rt–Rc trade-offs recorded for woody xeric species (Venegas-González et al., 2022; Rodríguez-Ramírez et al., 2022, 2024), likely mediated in *B. lutea* by wood anatomical adjustments that enhance hydraulic efficiency and reduce functional costs under high climatic variability.

During Super El Niño events, *B. lutea* exhibited reduced Rt but relatively high post-stress Rc, a pattern comparable to that reported for *Austrocedrus chilensis* (D. Don) Pic. Serm. & Bizzarri, *Nothofagus macrocarpa* (A. DC.) F.M. Vázquez & R.A. Rodr., *Cryptocarya alba* (Molina) Looser, and *Persea lingue* (Ruiz & Pav.) Nees (De Andrés et al., 2025; Gipoulou-Zúñiga et al., 2025). This response suggests that extreme climatic stress may temporarily constrain radial growth while allowing compensatory mechanisms (such as reserve reallocation, shifts in biomass allocation, or wood anatomical adjustments) to promote post-disturbance Rc, with outcomes strongly conditioned by species-specific traits and local environmental factors (Azócar et al., 2007; Guerra et al., 2024; Carabajo-Hidalgo et al., 2025). Consistent with this interpretation, higher Rs at San Pedro de Saños indicates a more effective re-establishment of growth following Super El Niño events, whereas lower Rs at Singua Chico may be associated with site-specific growth dynamics and the cumulative effects of recurrent ENSO-related stress (Rodriguez-Caton et al., 2021; Guerra et al., 2025; Zuidema et al., 2025).

Decline values (DecU = 0.110 in San Pedro de Saños; 0.160 in Singua Chico) indicate that *B. lutea* experiences a moderate reduction in post–Super El Niño radial growth, consistent with legacy physiological effects associated with combined thermal and hydric stress. This pattern may be linked to constraints on stomatal conductance, osmotic adjustment, and incomplete replenishment of non-structural carbohydrate reserves, ultimately delaying cambial reactivation under extreme conditions (Mu et al., 2022; Medeiros et al., 2025; Carabajo-Hidalgo et al., 2025). Comparable responses have been reported for *Quercus robur* L., *Carya palmeri* W.E. Manning, and *Carya myristiciformis* (F. Michx.) Nutt. exposed to prolonged droughts and thermal anomalies, highlighting the role of ecological memory in shaping post-stress growth dynamics (Gagen et al., 2019; Rodríguez-Ramírez et al., 2024). In this context, the near-null recovery observed in San Pedro de Saños (RecU ≈ 0) contrasts with the slightly positive recovery recorded in Singua Chico, potentially reflecting site-specific differences in pre-event water status, carbon storage

capacity, and early xylogenesis (phloem and/or xylem reactivation) (Hoch & Körner, 2005; Azócar et al., 2007; Jandova & Dolezal, 2025). Such variability in post-disturbance recovery is consistent with observations in other xeric woody species, where the timing and magnitude of growth resumption are tightly regulated by early-season water availability, cambial reactivation dynamics, and local microclimatic conditions (Gagen et al., 2019; Opała-Owczarek et al., 2024; Groenendijk et al., 2025; Zuidema et al., 2025).

Effects of Super El Niño events on wood anatomical traits

The wood anatomical traits correlated with Super El Niño events were key to understanding species-level responses by relating trait variations during Non-Super El Niño and Super El Niño events. We found links between specific traits and climate oscillations that could influence cambial initial cell length, reproduction, and survival. Past and current climatic variations could explain the observed individual correlations (Fig. 7). Many correlations between traits and Non-Super El Niño and Super El Niño events support generally accepted patterns, such as specific wood anatomical traits (D_H, V_L, F_{WW}, and F_{LT}) demonstrating a negative correlation with Super El Niño events.

These anatomical adjustments are mechanistically linked to the resilience indices calculated for *B. lutea*. Specifically, the reduction in vessel diameter (D_H) and vessel length (V_L) during Super El Niño events enhances hydraulic safety by minimizing the risk of cavitation under drought stress, which in turn supports higher resistance (Rt) by preventing complete hydraulic failure. The observed negative correlation of fiber wall width (F_{WW}) further indicates a shift toward stronger, more stress-tolerant xylem. After the extreme event ends, the ability to recover (Rc) is facilitated by the same anatomical traits: smaller vessels allow faster re-establishment of hydraulic conductivity with less carbon investment, which is consistent with the high Rc values recorded at both sites. Likewise, the moderate decline (DecU) and positive recovery (RecU) are directly explained by the plasticity of these wood anatomical traits, which enable *B. lutea* to balance hydraulic efficiency and safety under recurrent El Niño conditions. Thus, the resilience indices do not merely reflect radial growth dynamics; they are underpinned by quantifiable anatomical shifts that confer ecological memory and stress tolerance.

The study by Guerra et al. (2024) establishes a clear reference point for identifying climatic factors related to wood anatomical traits in Andean puna species. Their findings demonstrate significant correlations between traits such as vessel diameter (D_H) and vessel length (V_L) with climatic variables, particularly mean maximum temperature. This linkage supports using these wood anatomical traits as predictive markers for species' preferred habitats and potential responses to climate change. The strong trait-climate correlations highlight how slight climatic shifts could influence the ecological distribution and survival of these species in their high-altitude environments (Gipoulou-Zúñiga et al., 2025; Medeiros et al., 2025; Vieira et al., 2026).

The different ecological behaviors of wood anatomical traits are essential for ecological modeling. To better understand PAS, we need to develop broadly applicable methodologies that consider dendrometric, dendro-xylogenesis, and leaf vein traits. Some shrub species may develop enhanced resprouting abilities or clonal growth strategies to cope with more frequent disturbances, such as wildfires or droughts (Pratt et al., 2014; Gonzáles et al., 2024).

Revealing the relationships between traits and Super El Niño events in *Berberis* species will enhance our ability to predict the consequences of climate change. It is also important to consider that the specificity of shrub species in PAS, or conversely their resilience to extreme climatic events, serves as an ecological proxy for the probability of local extinction in these ecosystems (Sarikaya & Uzun, 2024; Ulloa et al., 2025; Vieira et al., 2026). Under- standing these relationships will also help us refine our predictions of the effects of ENSO events in xeric landscapes.

Conclusions

This study provides the first shrub-ring chronologies of *B. lutea* in the Peruvian altimontane shrublands, confirming its value as a reliable dendroecological proxy for high-elevation ecosystems with limited tree cover. Radial growth was mainly driven by temperature, evapotranspiration, and ENSO-related SST 3.4 variability, while precipitation played a more site-specific and seasonally restricted role. The contrasting responses between San Pedro de Saños and Singua Chico highlight the importance of local thermal and moisture conditions, as well as lagged climatic effects, in shaping shrub growth dynamics. The complexity of the precipitation–growth relationship in these altimontane ecosystems is reflected in the fact that, even in xeric sites, moisture is not always the primary driver, as evidenced by the negative correlation found at San Pedro de Saños. Despite the strong anomalies associated with Super El Niño events, *B. lutea* showed moderate resistance and rapid recovery, supported by reductions in vessel diameter that reflect a hydraulically safer strategy under

extreme stress. This anatomical plasticity may confer a survival advantage in a future with more frequent and intense Super El Niño events; however, scenarios of recurrent stress could exceed its recovery capacity. Overall, these findings position *B. lutea* as a sensitive climate archive and as a useful bioindicator for long-term monitoring of Andean ecosystem stability under global climate change, especially in the face of increasing extreme ENSO variability in high-elevation xeric ecosystems.

Acknowledgments

We extend our gratitude to park ranger Eber Melgar Guerra Almerco of the Reserva Paisajistica Nor Yauyos-Cochas (RPNYC) for his valuable assistance during field sampling. We also thank Fressia Ames-Martínez for her support in providing climatic data. In addition, we acknowledge the Plant Anatomy Laboratory of the Federal University of Lavras (Lavras, Brazil) and the Wood Anatomy Laboratory of Universidad Continental (Huancayo, Peru) for providing laboratory facilities for sample processing and analysis. Project supported by the Government of the State of Hidalgo through the Consejo de Ciencia, Tecnología e Innovación de Hidalgo (CITNOVA).

References

Aceituno P & Garreaud R (2016) The climate of the South American Altiplano. Oxford Research Encyclopedia of Climate Science. doi:10.1093/acrefore/9780190228620.013.977.

Andreu-Hayles L, Tejedor E, D'Arrigo R, Locosselli GM, Rodríguez-Catón M, Daux V, Oelkers R, Pacheco-Solana A, Paredes-Villanueva K & Rodríguez-Morata C (2023) Dendrochronological advances in the tropical and subtropical Americas: Research priorities and future directions. Dendrochronologia 81: 126124. doi:10.1016/j.dendro.2023.126124.

Azócar A, Rada F & García-Núñez C (2007) Functional characteristics of the arborescent genus Polylepis along a latitudinal gradient in the high Andes. Interciencia 32: 663–668.

Borcard D, Gillet F & Legendre P (2011) Numerical ecology with R. Springer New York, NY. doi:10.1007/978-1-4419-7976-6.

Briffa KR (1990) Basic chronology statistics and assessment. Methods of dendrochronology: applications in the environmental sciences. Kluwer Academic Publishers, Dordrecht, pp. 137–152.

Bruijnzeel LA, Mulligan M & Scatena FN (2011) Hydrometeorology of tropical montane cloud forests: emerging patterns. Hydrological Processes 25: 465–498. doi:10.1002/hyp.7974.

Bruijnzeel LA & Veneklaas EJ (1998) Climatic conditions and tropical montane forest productivity: The fog has not lifted yet. Ecology 79: 3–9. doi:10.1890/0012-9658(1998)079[0003:CCATMF]2.0.CO;2.

Bunn AG (2008) A dendrochronology program library in R (dplR). Dendrochronologia 26: 115–124. doi:10.1016/j.dendro.2008.01.002.

Cai W, McPhaden MJ, Grimm AM, Rodrigues RR, Taschetto AS, Garreaud RD, Dewitte B, Poveda G, Ham Y-G, Santoso A, Ng B, Anderson W, Wang G, Geng T, Jo H-S, Marengo JA, Alves LM, Osman M, Li S, Wu L, Karamperidou C, Takahashi K & Vera C (2020) Climate impacts of the El Niño–Southern Oscillation on South America. Nature Reviews Earth & Environment 1: 215–231. doi:10.1038/s43017-020-0040-3.

Carabajo-Hidalgo A, Nadal-Sala D, Poma B, Asbjornsen H, Crespo P & Sabaté S (2025) Cold and low irradiation shape *Polylepis reticulata*'s seasonal growth and water use dynamics at the Ecuadorian Andean tree line. Frontiers in Plant Science 16: 1675655. doi:10.3389/fpls.2025.1675655.

Carabajo-Hidalgo A, Sabaté S, Crespo P & Asbjornsen H (2023) Brief windows with more favorable atmospheric conditions explain patterns of *Polylepis reticulata* tree water use in a high-altitude Andean forest. Tree Physiology 43: 2085–2097. doi:10.1093/treephys/tpad109.

Carlquist S (1995) Wood anatomy of Berberidaceae: Ecological and phylogenetic considerations. Aliso 14: 85–103. doi:10.5642/aliso.19951402.03.

Coaguila L, Mataix-Solera J, Nina S, García-Carmona M & Salazar ET (2025) Soil degradation evidence following a wildfire in Arequipa's Andean region, Peru. Spanish Journal of Soil Science 15: 13983. doi:10.3389/sjss.2025.13983.

Crispín-DelaCruz DB, Morales MarianoS, Andreu-Hayles Laia, Christie DuncanA, Guerra A & Requena-Rojas EdilsonJ (2022) High ENSO sensitivity in tree rings from a northern population of *Polylepis tarapacana* in the Peruvian Andes. Dendrochronologia 71: 125902. doi:10.1016/j.dendro.2021.125902.

De Andrés EG, Fajardo A, Camarero JJ, Fernández-Cortés Á & Gazol A (2025) Surviving a megadrought: shifts in climate sensitivity of an austral conifer in Chile due to persistent water shortage. Agricultural and Forest Meteorology 373: 110791. doi:10.1016/j.agrformet.2025.110791.

De Moura GS, Da Silva AC, Da Silva Lima BL, Hassan VOC, Da Rocha Reis LV, Oliveira CV & Higuchi P (2025) Fog and moisture conditions modulate the effect of temperature on radial growth of an endemic cloud forest tree. Plant Ecology 226: 1017–1023. doi:10.1007/s11258-025-01548-4.

Dobbert S, Albrecht EC, Pape R & Löffler J (2022) Alpine shrub growth follows bimodal seasonal patterns across biomes – unexpected environmental controls. Communications Biology 5: 793. doi:10.1038/s42003-022-03741-x.

Dray S & Dufour AB (2007) The ade4 package: Implementing the duality diagram for ecologists. Journal of Statistical Software 22. doi:10.18637/jss.v022.i04.

Dusenge ME, González Caro S, Restrepo Z, Gardner A, Meir P, Hartley IP, Sitch S, Sanchez A, Villegas JC & Mercado LM (2025) Unexpected large photosynthetic thermal plasticity of montane andean trees. Global Change Biology 31: e70266. doi:10.1111/gcb.70266.

Feng X, Ding Q, Wu L, Jones C, Baxter I, Tardif R, Stevenson S, Emile-Geay J, Mitchell J, Carvalho LMV, Wang H & Steig EJ (2021) A multidecadal-scale tropically driven global teleconnection over the past millennium and its recent strengthening. Journal of Climate 34: 2549–2565. doi:10.1175/JCLI-D-20-0216.1.

Feron S, Cordero RR, Damiani A, MacDonell S, Pizarro J, Goubanova K, Valenzuela R, Wang C, Rester L & Beaulieu A (2024) South America is becoming warmer, drier, and more flammable. Communications Earth & Environment 5: 501. doi:10.1038/s43247-024-01654-7.

Fonti MV, Von Arx G, Harroue M, Schneider L, Nievergelt D, Björklund J, Hantemirov R, Kukarskih V, Rathgeber CBK, Studer N-T & Fonti P (2025) A protocol for high-quality sectioning for tree-ring anatomy. Frontiers in Plant Science 16: 1505389. doi:10.3389/fpls.2025.1505389.

Franklin GL (1945) Preparation of thin sections of synthetic resins and wood-resin composites, and a new macerating method for wood. Nature 155: 51–51. doi:10.1038/155051a0.

Fritts H (1976) Tree rings and climate. Academic Press, London.

Gagen M, Matthews N, Denman S, Bridge M, Peace A, Pike R & Young G (2019) The tree ring growth histories of UK native oaks as a tool for investigating Chronic Oak Decline: An example from the Forest of Dean. Dendrochronologia 55: 50–59. doi:10.1016/j.dendro.2019.03.001.

Ganthaler A & Mayr S (2021) Subalpine dwarf shrubs differ in vulnerability to xylem cavitation: An innovative staining approach enables new insights. Physiologia Plantarum 172: 2011–2021. doi:10.1111/ppl.13429.

García-Plazaola JI, Rojas R, Christie DA & Coopman RE (2015) Photosynthetic responses of trees in high-elevation forests: comparing evergreen species along an elevation gradient in the Central Andes. AoB Plants 7: plv058. doi:10.1093/aobpla/plv058.

Gipoulou-Zúñiga T, Rojas-Badilla M, LeQuesne C & Rozas V (2025) Endemic threatened tree species in the Mediterranean forests of central Chile are highly sensitive to ENSO-driven water availability and drought. Forest Ecosystems 13: 100324. doi:10.1016/j.fecs.2025.100324.

Gonzáles H, Ocaña CL, Cubas JA, Vega-Nieva DJ, Ruíz M, Santos A & Barboza E (2024) Impact of forest fire severity on soil physical and chemical properties in pine and scrub forests in high Andean zones of Peru. Trees, Forests and People 18: 100659. doi:10.1016/j.tfp.2024.100659.

Graham EA, Mulkey SS, Kitajima K, Phillips NG & Wright SJ (2003) Cloud cover limits net CO_2 uptake and growth of a rainforest tree during tropical rainy seasons. Proceedings of the National Academy of Sciences 100: 572–576. doi:10.1073/pnas.0133045100.

Grissino-Mayer HD (2001) Evaluating crossdating accuracy: a manual and tutorial for the computer program COFECHA. Tree-Ring Research 57: 205–221.

Groenendijk P, Babst F, Trouet V, Fan Z-X, Granato-Souza D, Locosselli GM, Mokria M, Panthi S, Pumijumnong N, Abiyu A, Acuña-Soto R, Adenesky-Filho E, Alfaro-Sánchez R, Anholetto Junior CR, Aragão JRV, Assis-Pereira G, Astudillo-Sánchez CC, Carolina Barbosa A, Barreto NDO, Battipaglia G, Beeckman H, Botosso PC, Bourland N, Bräuning A, Brienen R, Brookhouse M, Buajan S, Buckley BM, Camarero JJ, Carrillo-Parra A, Ceccantini G, Centeno-Erguera LR, Cerano-Paredes J, Cervantes-Martínez R, Chanthorn W, Chen Y-J, Cintra BBL, Cornejo-Oviedo EH, Cortés-Cortés O, Costa CM, Couralet C, Crispin-DelaCruz DB, D'Arrigo R, David DA, De Ridder M, Del Valle JI, Díaz-Carrillo OA, Dobner Jr M, Doucet J-L, Dünisch O, Enquist BJ, Esemann-Quadros K, Esquivel-Arriaga G, Fayolle A, Fenilli TAB, Ferrero ME, Fichtler E, Finnegan PM, Fontana C, Francisco KS, Fu P-L, Galvão F, Gebrekirstos A, Giraldo JA, Gloor E, Godoy-Veiga M, Guerra A, Haneca K, Harley GL, Heinrich I, Helle G, Hernández-Díaz JC, Hornink B, Hubau W, Inga JG, Islam M, Jiang Y, Kaib M, Hassan Khamisi Z, Koprowski M, Layme E, Leffler AJ, Ligot G, Lisi CS, Loader NJ, Lobo FDA, Longhi-Santos T, Lopez L, López-Hernández MI, Lousada JLPC, Manzanedo RD, Marcon AK, Maxwell JT, Mendivelso HA, Mendoza-Villa ON, Menezes ÍRN, Montóia VR, Moors E, Moreno M, Muñiz-Castro MA, Nabais C, Nathalang A, Ngoma J, Nogueira Jr. FDC, Oliveira JM, Olmedo GM, Ortega-Rodriguez DR, Ortíz CER, Pagotto MA, Paredes-Villanueva K, Pérez-De-Lis G, Ponce Calderón LP, Portal-Cahuana LA, Pucha-Cofrep DA, Quadri P, Rahman M, Ramírez JA, Requena-Rojas EJ, Reyes-Flores J, Ribeiro ADS, Robert-

son I, Roig FA, Roquette JG, Rubio-Camacho EA, Sánchez-Salguero R, Sass-Klaassen U, Schöngart J, Scipioni MC, Sheppard PR, Silva LCR, Slotta F, Soria-Díaz L, Sousa LKVS, Speer JH, Therrell MD, Ticse-Otarola G, Tomazello-Filho M, Torbenson MCA, Tor-Ngern P, Touchan R, Van Den Bulcke J, Vázquez-Selem L, Velázquez-Pérez AH, Venegas-González A, Villalba R, Villanueva-Diaz J, Vlam M, Vourlitis G, Wehenkel C, Wils T, Zavaleta ES, Zewdu EA, Zhang Y-J, Zhou Z-K & Zuidema PA (2025) The importance of tropical tree-ring chronologies for global change research. Quaternary Science Reviews 355: 109233. doi:10.1016/j.quascirev.2025.109233.

Guerra A, Ames-Martínez FN, Crispín-DelaCruz DB, Orellana-Mendoza E, Requena-Rojas EJ & Rodríguez-Ramírez EC (2025) Polylepis wood acclimation strategies to ENSO events. Scientific Reports 15: 19236. doi:10.1038/s41598-025-04422-5.

Guerra A, Ames-Martínez FN & Rodríguez-Ramírez EC (2024) Wood anatomical acclimation in the endemic genus *Polylepis* in Peruvian Andean forests. Journal of Mountain Science 21: 2986–3000. doi:10.1007/s11629-024-8738-1.

Hadad M, Flores D, Gallardo V, Roig FA, González-Reyes Á & Chen F (2022) Dendroclimatic potential of the *Adesmia pinifolia* shrub growing at high altitude in the Andes foothills. Dendrochronologia 72: 125919. doi:10.1016/j.dendro.2021.125919.

Hoch G & Körner C (2005) Growth, demography and carbon relations of *Polylepis* trees at the world's highest treeline. Functional Ecology 19: 941–951. doi:10.1111/j.1365-2435.2005.01040.x.

Holmes RL (1983) Computer-assisted quality control in tree-ring dating and measurement. Tree-Ring Bulletin 43: 69–78.

Holmgren M, Stapp P, Dickman CR, Gracia C, Graham S, Gutiérrez JR, Hice C, Jaksic F, Kelt DA, Letnic M, Lima M, López BC, Meserve PL, Milstead WB, Polis GA, Previtali MA, Richter M, Sabaté S & Squeo FA (2006) Extreme climatic events shape arid and semiarid ecosystems. Frontiers in Ecology and the Environment 4: 87–95. doi:10.1890/1540-9295(2006)004[0087:ECESAA]2.0.CO;2.

Hughes NM, Sanchez A, Berry ZC & Smith WK (2024) Clouds and plant ecophysiology: missing links for understanding climate change impacts. Frontiers in Forests and Global Change 7: 1330561. doi:10.3389/ffgc.2024.1330561.

IAWA Committee (1989) IAWA list of microscopic features for hardwood identification. IAWA Journal.

Jandova V & Dolezal J (2025) Ontogenetic shifts in biomass allocation and xylem structure of the world's highest-occurring plants: balancing growth, storage, and resilience in the extreme Himalayan subnival zone. Plant Biology 27: 1176–1186. doi:10.1111/plb.70045.

Karger DN, Lange S, Hari C, Reyer CP & Zimmermann NE (2021) CHELSA-W5E5 v1. 0: W5E5 v1. 0 downscaled with CHELSA v2. 0. doi:10.48364/ISIMIP.836809.1.

Körner C (2012) Treelines will be understood once the functional difference between a tree and a shrub is. AMBIO 41: 197–206. doi:10.1007/s13280-012-0313-2.

Körner C (2021) The cold range limit of trees. Trends in Ecology & Evolution 36: 979–989. doi:10.1016/j.tree.2021.06.011.

Lyu Y, Li Y, Tang X, Wang F & Wang J (2018) Contrasting intraseasonal variations of the equatorial pacific ocean Between the 1997–1998 and 2015–2016 El Niño events. Geophysical Research Letters 45: 9748–9756. doi:10.1029/2018GL078915.

Macek P, Macková J & de Bello F (2009) Morphological and ecophysiological traits shaping altitudinal distribution of three *Polylepis* treeline species in the dry tropical Andes. Acta Oecologica 35: 778–785. doi:10.1016/j.actao.2009.08.013.

Magnússon RÍ, Sass Klaassen U, Limpens J, Karsanaev SV, Ras S, Van Huissteden K, Blok D & Heijmans MMPD (2023) Spatiotemporal variability in precipitation growth association of *Betula nana* in the Siberian lowland tundra. Journal of Ecology 111: 1882–1904. doi:10.1111/1365-2745.14165.

McCracken E & Johansen DA (1940) Plant microtechnique. McGraw-Hill, New York.

Medeiros CD, Trueba S, Henry C, Fletcher LR, Lutz JA, Méndez Alonzo R, Kraft NJB & Sack L (2025) Simplification of woody plant trait networks among communities along a climatic aridity gradient. Journal of Ecology 113: 896–912. doi:10.1111/1365-2745.70010.

Melián EA, Hadad M, Flores D, Gallardo V, Ribas Y, Romero E & Roig F (2024) Evaluación del potencial dendrocronológico de dos arbustos que coexisten en áreas desérticas de montaña del centro-oeste de Argentina. Darwiniana, nueva serie 12: 107–121. doi:10.14522/darwiniana.2024.121.1200.

Morales MS, Crispín-DelaCruz DB, Álvarez C, Christie DA, Ferrero ME, Andreu-Hayles L, Villalba R, Guerra A, Ticse-Otarola G, Rodríguez-Ramírez EC, LLocclla-Martínez R, Sanchez-Ferrer J & Requena-Rojas EJ (2023) Drought increase since the mid-20th century in the northern South American Altiplano revealed by a 389-year precipitation record. Climate of the Past 19: 457–476. doi:10.5194/cp-19-457-2023.

Mosquera GM, Marín F, Carabajo-Hidalgo A, Asbjornsen H, Célleri R & Crespo A (2024) Ecohydrological assessment of the water balance of the world's highest elevation tropical forest (*Polylep-*

is). Science of the Total Environment 941: 173671. doi:10.1016/j.scitotenv.2024.173671.

Mu Y, Lyu L, Li Y & Fang O (2022) Tree-ring evidence of ecological stress memory. Proceedings of the Royal Society B 289: 20221850. doi:10.1098/rspb.2022.1850.

Oksanen J, Simpson GL, Blanchet FG, Kindt R, Legendre P, Minchin PR, O'Hara RB, Solymos P, Stevens MHH, Wagner H, Barbour M, Bedward M, Bolker B, Borcard D, Borman T, Carvalho G, Chirico M, De Caceres M, Durand S, Evangelista HBA, FitzJohn R, Friendly M, Furneaux B, Hannigan G, Hill MO, Lahti L, Martino C, McGlinn D, Ouellette M-H, Ribeiro Cunha E, Smith T, Stier A, Ter Braak CJF & Weedon J (2019) vegan: community ecology package. R package version 2.4-7.

Oladi R, Emaminasab M & Eckstein D (2017) The dendroecological potential of shrubs in north Iranian semi-deserts. Dendrochronologia 44: 94–102. doi:10.1016/j.dendro.2017.04.004.

Opała-Owczarek M, Owczarek P, Phulara M, Bielec-Bąkowska Z & Wawrzyniak Z (2024) Dendrochronology and extreme climate signals recorded in seven Icelandic shrubs: A multi-species approach in the sub-Arctic. Dendrochronologia 85: 126207. doi:10.1016/j.dendro.2024.126207.

Orvis KH & Grissino-Mayer HD (2002) Standardizing the reporting of abrasive papers used to surface tree-ring samples. Tree-Ring Research 58: 47–50.

Peel MC, Finlayson BL & McMahon TA (2007) Updated world map of the Köppen-Geige climate classification. Hydrology and Earth System Sciences 11: 1633–1644. doi:10.5194/hess-11-1633-2007.

Portal-Cahuana LA, Fontana C, Assis-Pereira G, Groenendijk P, Roig FA & Tomazello-Filho M (2023) Thirty-four years of dendrochronological studies in Perú: A review of advances and challenges. Dendrochronologia 78: 126058. doi:10.1016/j.dendro.2023.126058.

Poveda G, Espinoza JC, Zuluaga MD, Solman SA, Garreaud R & Van Oevelen PJ (2020) High impact weather events in the Andes. Frontiers in Earth Science 8: 162. doi:10.3389/feart.2020.00162.

Pratt RB, Jacobsen AL, Ramirez AR, Helms AM, Traugh CA, Tobin MF, Heffner MS & Davis SD (2014) Mortality of resprouting chaparral shrubs after a fire and during a record drought: physiological mechanisms and demographic consequences. Global Change Biology 20: 893–907. doi:10.1111/gcb.12477.

Pumijumnong N, Muangsong C, Buajan S, Songtrirat P, Chatwatthana R & Chareonwong U (2023) Factors Affecting Cambial Growth Periodicity and Wood Formation in Tropical Forest Trees: A Review. Forests 14: 1025. doi:10.3390/f14051025.

Richter M & Ise M (2005) Monitoring plant development after El Niño 1997/98 in northwestern Perú. Erdkunde 59: 136–155.

Rifai SW, Li S & Malhi Y (2019) Coupling of El Niño events and long-term warming leads to pervasive climate extremes in the terrestrial tropics. Environmental Research Letters 14: 105002. doi:10.1088/1748-9326/ab402f.

Rodriguez-Caton M, Andreu-Hayles L, Morales MS, Daux V, Christie DA, Coopman RE, Alvarez C, Rao MP, Aliste D, Flores F & Villalba R (2021) Different climate sensitivity for radial growth, but uniform for tree-ring stable isotopes along an aridity gradient in *Polylepis tarapacana*, the world's highest elevation tree species (ed. by L Cernusak) Tree Physiology 41: 1353–1371. doi:10.1093/treephys/tpab021.

Rodríguez-Morata C, Pacheco-Solana A, Ticse-Otarola G, Boza Espinoza TE, Crispín-DelaCruz DB, Santos GM, Morales MS, Requena-Rojas EJ & Andreu-Hayles L (2022) Revealing Polylepis microphylla as a suitable tree species for dendrochronology and quantitative wood anatomy in the Andean montane forests. Dendrochronologia 76: 125995. doi:10.1016/j.dendro.2022.125995.

Rodríguez-Ramírez EC, Ferrero ME, Acevedo-Vega I, Crispin-DelaCruz DB, Ticse-Otarola G & Requena-Rojas EJ (2022) Plastic adjustments in xylem vessel traits to drought events in three *Cedrela* species from Peruvian Tropical Andean forests. Scientific Reports 12: 21112. doi:10.1038/s41598-022-25645-w.

Rodríguez-Ramírez EC, Frei J, Ames-Martínez FN, Guerra A & Andrés-Hernández AR (2024) Ecological stress memory in wood architecture of two Neotropical hickory species from central-eastern Mexico. BMC Plant Biology 24: 638. doi:10.1186/s12870-024-05348-2.

Ruiz-Valencia JA, Andrés-Hernández AR & Terrazas T (2022) Anatomía de la madera de nueve especies de la selva baja caducifolia en la Sierra del Tentzo, Puebla, México 129. Acta Botanica Mexicana. doi:10.21829/abm129.2022.2076.

Sahney M & Tripathi N (2020) Wood anatomy (stem and root) of *Berberis lycium* Royle (Berberidaceae) and its ecological adaptation. Indian Journal of Plant Sciences 9: 91–98.

Sánchez-Calderón OD, Carlón-Allende T, Mendoza ME & Villanueva-Díaz J (2022) Dendroclimatology in Latin America: A review of the state of the art. Atmosphere 13: 748. doi:10.3390/atmos13050748.

Sarikaya AG & Uzun A (2024) Modeling the effects of climate change on the current and future potential distribution of *Berberis vulgaris* L. with machine learning. Sustainability 16: 1230. doi:10.3390/su16031230.

Schulman E (1956) Dendroclimatic changes in semiarid America. University of Arizona Press.

Speer JH (2010) Fundamentals of tree-ring research. University of Arizona Press.

Suárez E, Encalada AC, Chimbolema S, Jaramillo R, Hofstede R & Riveros-Iregui D (2023) On the use of "Alpine" for high-elevation tropical environments. Mountain Research and Development 43: 1–4. doi:10.1659/mrd.2022.00024.

Taschetto AS, Ummenhofer CC, Stuecker MF, Dommenget D, Ashok K, Rodrigues RR & Yeh S (2020) ENSO atmospheric teleconnections. Geophysical Monograph Series (ed by MJ McPhaden, A Santoso & W Cai) 1st edn. Wiley, pp. 309–335. doi:10.1002/9781119548164.ch14.

Trouet V & Van GJ (2013) KNMI climate explorer: a web-based research tool for high-resolution paleoclimatology. Tree-Ring Research 69: 3–13. doi:10.3959/1536-1098-69.1.3.

Ulloa C, Sagástegui A & Sánchez I (2006) Berberidaceae endémicas del Perú. Revista Peruana de Biología 13: 171–173. doi:10.15381/rpb.v13i2.1811.

Ulloa C, Sánchez-Lara E & Oleas N (2025) Conservation profile of endemic species of *Berberis* from Ecuador (Berberidaceae, Ranunculales). Biodiversity Data Journal 13: e157827. doi:10.3897/BDJ.13.e157827.

Venegas-González A, Gibson-Capintero S, Anholetto-Junior C, Mathiasen P, Premoli AC & Fresia P (2022) Tree-ring analysis and genetic associations help to understand drought sensitivity in the Chilean endemic forest of *Nothofagus macrocarpa*. Frontiers in Forests and Global Change 5: 762347. doi:10.3389/ffgc.2022.762347.

Vieira P, Mulligan M, Adrian Bruijnzeel L, Pires-Oliveira JC, Ponette-González AG, Brauman KA, Eisenlohr PV, Flörke M, Leite Fontes MA, Petry P & Da Rocha HR (2026) Most South American cloud forests are likely to disappear under high-end climate change. Journal for Nature Conservation 90: 127192. doi:10.1016/j.jnc.2025.127192.

Wang Y, Naumann U, Wright ST & Warton DI (2012) mvabund– an R package for model-based analysis of multivariate abundance data. Methods in Ecology and Evolution 3: 471–474. doi:10.1111/j.2041-210X.2012.00190.x.

Warton DI, Shipley B & Hastie T (2015) CATS regression – a model-based approach to studying trait-based community assembly (ed. by RB O'Hara) Methods in Ecology and Evolution 6: 389–398. doi:10.1111/2041-210X.12280.

Wei T & Simko V (2010) corrplot: visualization of a correlation matrix. R package version 0.92.

Wickham H, Chang W & Wickham MH (2021) ggplot2: create elegant data visualizations using the grammar of graphics. R package.

Wigley TML, Briffa KR & Jones PD (1984) On the average value of correlated time series, with applications in dendroclimatology and hydrometeorology. Journal of Applied Meteorology and Climatology 23: 201–213. doi:10.1175/1520-0450(1984)023<0201:OTAVOC>2.0.CO;2.

Wilson AM & Jetz W (2016) Remotely sensed high-resolution global cloud dynamics for predicting ecosystem and biodiversity distributions (ed. by M Loreau) PLOS Biology 14: e1002415. doi:10.1371/journal.pbio.1002415.

Zuidema PA, Groenendijk P, Rahman M, Trouet V, Abiyu A, Acuña-Soto R, Adenesky-Filho E, Alfaro-Sánchez R, Anholetto CR, Aragão JRV, Assis-Pereira G, Astudillo-Sánchez CC, Barbosa AC, Battipaglia G, Beeckman H, Botosso PC, Bourland N, Bräuning A, Brienen R, Brookhouse M, Buajan S, Buckley BM, Camarero JJ, Carrillo-Parra A, Ceccantini G, Centeno-Erguera LR, Cerano-Paredes J, Cervantes-Martínez R, Chanthorn W, Chen Y-J, Cintra BBL, Cornejo-Oviedo EH, Cortés-Cortés O, Costa CM, Couralet C, Crispín-De-La-Cruz DB, D'arrigo R, David DA, De Ridder M, Del Valle JI, Dobner M, Doucet J-L, Dünisch O, Enquist BJ, Esemann-Quadros K, Esquivel-Arriaga G, Fan Z-X, Fayolle A, Fenilli TAB, Ferrero ME, Fichtler E, Finnegan PM, Fontana C, Francisco KS, Fu P-L, Galvão F, Gebrekirstos A, Giraldo JA, Gloor E, Godoy-Veiga M, Granato-Souza D, Guerra A, Haneca K, Harley GL, Heinrich I, Helle G, Hornink B, Hubau W, Inga JG, Islam M, Jiang Y-M, Kaib M, Khamisi ZH, Koprowski M, Layme E, Leffler AJ, Ligot G, Lisi CS, Loader NJ, Lobo FDA, Locosselli GM, Longhi-Santos T, Lopez L, López-Hernández MI, Lousada JLPC, Manzanedo RD, Marcon AK, Maxwell JT, Mendoza-Villa ON, Nunes Menezes ÍR, Mokria M, Montóia VR, Moors E, Moreno M, Muñiz-Castro MA, Nabais C, Nathalang A, Ngoma J, Nogueira FDC, Oliveira JM, Olmedo GM, Ortega-Rodriguez DR, Rodríguez Ortíz CE, Pagotto MA, Panthi S, Paredes-Villanueva K, Pérez-de-Lis G, Calderón LPP, Portal-Cahuana LA, Pucha-Cofrep DA, Pumijumnong N, Quadri P, Ramírez JA, Requena-Rojas EJ, Reyes-Flores J, Ribeiro ADS, Robertson I, Roig FA, Roquette JG, Rubio-Camacho EA, Sánchez-Salguero R, Sass-Klaassen U, Schöngart J, Scipioni MC, Sheppard PR, Silva LCR, Slotta F, Soria-Díaz L, Sousa LKVS, Speer JH, Therrell MD, Ticse-Otarola G, Tomazello-Filho M, Torbenson MCA, Tor-Ngern P, Touchan R, Van Den Bulcke J, Vázquez-Selem L, Velázquez-Pérez AH, Venegas-González A, Villalba R, Villanueva-Diaz J, Vlam M, Vourlitis G, Wehenkel C, Wils T, Zavaleta ES, Zewdu EA, Zhang Y-J, Zhou Z-K & Babst F (2025) Pantropical tree rings show small effects of drought on stem growth. Science 389: 532–538. doi:10.1126/science.adq6607.